CRYSTAL GROWTH & DESIGN

Article

pubs.acs.org/crystal

TiO_2 Nanorod-Derived Synthesis of Upstanding Hexagonal Kassite Nanosheet Arrays: An Intermediate Route to Novel Nanoporous TiO_2 Nanosheet Arrays

Xiaoyan Gan,*[,†] Xiangdong Gao,[†] Jijun Qiu,[†] Peng He,[†,‡] Xiaomin Li,[†] and Xiudi Xiao[§]

[†]State Key Laboratory of High Performance Ceramics and Superfine Microstructures, Shanghai Institute of Ceramics, Chinese Academy of Sciences, 1295 Ding Xi Road, Shanghai, 200050, People's Republic of China

[‡]Graduate School of the Chinese Academy of Sciences, People's Republic of China

[§]Key Laboratory of Renewable Energy and Gas Hydrates, Guangzhou Institute of Energy Conversion, Chinese Academy of Sciences, No. 2 Nengyuan Road, Wushan, Tianhe District, Guangzhou, 510640, People's Republic of China

Supporting Information

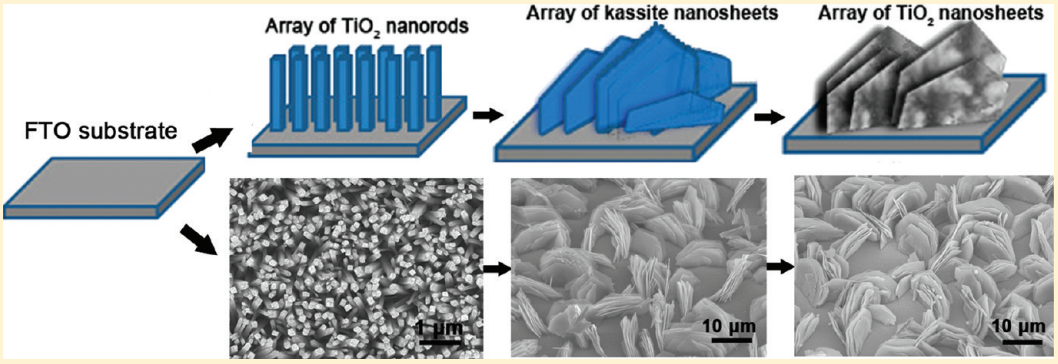

ABSTRACT: In this report, upstanding and nanoporous hexagonal TiO_2 nanosheet arrays were achieved via using kassite [$CaTi_2O_4(OH)_2$] as an intermediate. The process developed involved a TiO_2 nanorod-derived synthesis of upstanding hexagonal kassite nanosheet arrays and a transformation of the kassite to TiO_2. To the best of our knowledge, this is the first successful attempt to grow ordered hexagonal kassite nanosheet arrays. The as-obtained kassite nanosheets showed a single-crystalline nature with their *c*-axis parallel to the substrate. A stepwise study of the growth of the interesting hexagonal kassite nanosheet arrays was demonstrated. Upon hydrothermal treatment with diluted HNO_3 aqueous solution, the single-crystalline hexagonal kassite got converted to nanoporous rutile TiO_2, with shape preservation. The approach described in this study provides a novel method for the synthesis of kassite and TiO_2 nanosheet arrays and are ready for a variety of applications such as in catalytic or optoelectronic fields.

1. INTRODUCTION

Nanostructured metal-oxide semiconductors have attracted great attention in recent years due to their exceptional electronic, optical, chemical, and mechanical properties. Among the various metal-oxide semiconductors, the well-known nanostructured TiO_2 can still offer unexplored opportunities in applications related to environmental cleaning and protection,[1] photocatalysis,[2] gas-sensing,[3] lithium ion batteries,[4] and solar cells.[5] Mainly, three approaches including hydrothermal or solvethermal reaction,[4,6] template synthesis,[7,8] and electrospin[9] have been reported for preparing TiO_2-based nanotubes, nanowires, nanosheets, or nanofibers in powdery form. However, well-organized and oriented TiO_2 nanostructure arrays properly adhering to the substrate are often more desirable for applications involving catalysis, sensing, photovoltaic cells, and high-surface area electrodes. Extensive efforts have been devoted to the fabrication of arrays of ordered TiO_2 nanostructures in recent years,[10−18] pursuing the profits on large internal surface area, optimal exposure of the sample surface to the environment, and direct electron transport passway. A number of synthesis techniques have been used to synthesize oriented TiO_2 nanowires or nanotubes arrays, such as template sol−gel methods,[10] high temperature chemical vapor deposition,[11,12] transformation from titanate,[13−15] and anodic oxidation.[16,17] In general, these TiO_2 nanostructure arrays were limited to non-transparent (Ti foils[13−16]) or nonconductive (AAO template[10]) substrates or Ti[18] or Au-coated transparent conducting oxide (TCO) substrate.[11,12] The facile and cost-effective fabrication of well-aligned TiO_2-based nanostructure arrays on TCO substrates remains a great challenge.

Received: August 15, 2011
Revised: November 9, 2011
Published: November 15, 2011

   dx.doi.org/10.1021/cg2010612 | *Cryst. Growth Des.* 2012, 12, 289−296

Scheme 1. Overall Strategy toward 2D TiO_2 Nanosheet Arrays, Involving a Direct Hydrothermal Deposition of Vertically Aligned TiO_2 Nanorods on FTO Glass Substrate, a Deviation of These TiO_2 Nanorods to Hexagonal Kassite Nanosheet Arrays and a Final Transformation of Kassite Arrays to TiO_2 Nanosheet Arrays

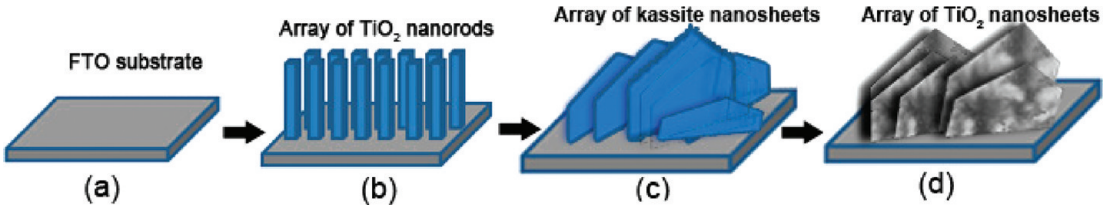

Recently, Qiu et al.[18] and Xu et al.[19] prepared ordered TiO_2 nanotube arrays on TCO substrates from a solution method by taking ZnO nanowire as a template. Feng et al.[20] and Liu et al.[21] developed a simple hydrothermal method to grow oriented single-crystalline TiO_2 nanowires directly on F-doped tin oxide (FTO) glass substrate and showed a remarkable conversion efficiency of the TiO_2 nanowire arrays in dye-sensitized solar cells. While all of the above-mentioned references have focused on the fabrication of 1D TiO_2 nanostucure arrays, there have been hardly any investigations that address the 2D TiO_2 arrays to date. Herein, we report for the first time a wet-chemical synthesis of 2D TiO_2 arrays on FTO glass substrates, in which calcium titanate [kassite, $CaTi_2O_4(OH)_2$] arrays nanosheets were used as an intermediate to further produce 2D TiO_2 arrays. Kassite, which was seldom produced artificially in the literature, was considered as a layered metal hydroxide that converted to $CaTiO_3$ by calcinations.[22] So far, to the best of our knowledge, the chemical synthesis of kassite nanosheet arrays and their utilization as intermediate to prepare TiO_2 nanostructure rarely has been investigated. The overall strategy is illustrated in Scheme 1, involving a direct hydrothermal deposition of vertically aligned TiO_2 nanorods on FTO glass substrate, a deviation of these TiO_2 nanorods to hexagonal kassite nanosheet arrays, and a final transformation of the kassite arrays to TiO_2 nanosheet arrays. The specific advantage of our method is that it provides well-aligned 2D sheetlike arrays of kassite [$CaTi_2O_4(OH)_2$] and TiO_2 nanorods on FTO glass substrate, both of which have promising application in catalysts and electroactive or photoactive materials in the future.

2. EXPERIMENTAL DETAILS

The following commercial reagents were purchased from Sinopharm Chemical Reagent Cor. Ltd. and used directly without further purification: tetrabutyl titanate (98%), hydrochloric acid (37%), sodium hydroxide (96%), and nitric acid (65−68%). Prior to the synthesizing, the FTO substrates were ultrasonically cleaned in acetone, ethanol, and deionized water for 5 min, respectively. The substrates were then placed upside down in a Teflon-lined stainless steel autoclave (100 mL), containing 30 mL of deionized water, 30 mL of hydrochloric acid (37 wt %), and 0.8 mL of tetrabutyl titanate. The autoclave was placed and kept in an oven for 10 h at 150 °C. The reactor was then cooled rapidly to room temperature under flowing water. The substrates were removed from the reactor, rinsed, and dried. TiO_2 nanorod arrays were obtained on the substrate. The TiO_2 nanorod arrays were then dipped into 15 mL of 10 M NaOH solution in a sealed Teflon reactor and autoclaved at 150 °C for different duration (1−8 h). The samples were then washed thoroughly with deionized water to remove any traces of NaOH and dried. The resulting sample after reacting with alkaline solution for 5 h was further dipped into 0.1 M HNO_3 aqueous solution and autoclaved at 150 °C for 7 h to convert to TiO_2.

X-ray diffraction (XRD; Cu Kα, RIGAKU, D/MAX-2550 V), glancing angle XRD with a glancing angle of 1° (GAXRD: Cu Kα), field emission scanning electron microscope (FESEM; S-4700, Hitachi, operating voltage: 10 kV), and transmission electron microscopy equipped with selected area electron diffraction were employed (TEM/SAED; JEM200CX, operated at 200 kV) to characterize the crystal structure and morphology of the samples. Raman spectra were recorded at room temperature by a Jobin Yvon LabRAM HR 800UV micro-Raman system under an Ar+ (514.5 nm) laser excitation.

3. RESULTS AND DISCUSSION

Figure 1a,b shows representative SEM images of the TiO_2 nanorod arrays synthesized from a 0.8 mL of tetrabutyl titanate and 60 mL of hydrochloric acid (18.5 wt %) mixed solution under hydrothermal condition at 150 °C for 18 h. Vertically aligned nanorod arrays with square cross-sections were uniformly formed on a large scale on FTO substrate. Their average length and diameter were 2 μm and 110 nm, respectively. The corresponding XRD pattern (Figure 1c) of the nanorod arrays completely matched with the tetragonal rutile phase of titania (JCPDS card: 86-0147). The enhanced (002) peak indicated that the nanorods grew perpendicular to the substrate, which agreed well with results from the SEM images. Figure 1d shows the TEM image of nanorod with a diameter of 100 nm. Its corresponding SAED pattern (inserted in Figure 1d) indicated that the nanorod was single-crystalline and grew along the ⟨001⟩ direction, which were consistent with those from the SEM and XRD results.

Figure 2a−c display titled- and side-view of typical 2D hexagonal nanosheet arrays on FTO substrate obtained by treating the TiO_2 arrays in 10 M NaOH solution at 150 °C for 5 h. As shown in Figure 2a−c, a large quantity of hexagonal nanosheets, which stood upward, were observed on the substrate, demonstrating very good uniformity. The hexagonal nanosheets were about 12 μm in diameter and 200−300 nm in thickness and had a smooth surface. The nanosheets appeared to be stacked layerwise, forming a multilayer platelet structure. The corresponding XRD pattern of the multilayer nanosheet arrays is shown in Figure 2d. It revealed that besides diffraction peaks from FTO substrate, peaks that were denoted by solid square appeared at 2θ = 19.5, 27.1, 34.1, 39.1, 39.5, 44.2, 56.9, and 61.0°. These diffraction peaks resembled those of the kassite structure (JCPDS: 88-1722, hexagonal, $a = b$ = 0.542 nm, and c = 0.468 nm) but had a slight shift and split peaks. The marked peaks matched well with those of the kassite structure reported by Huang et al.[22] According to the Rietveld refinement by Huang et al,[22] the artificially synthesized kassite, chemically formulated as $CaTi_2O_4(OH)_2$, was hexagonal with lattice constants of $a = b$ = 0.5245 nm, and c = 0.4784 nm. The enhanced diffraction peak at 2θ = 19.5°, which should be indexed to the {100} plane, indicated that the platelets were ⟨100⟩-oriented, agreeing well with the SEM images in Figure 2a−c. It was worthwhile to note that the hexagonal nanosheet morphology of $CaTi_2O_4(OH)_2$ should be ascribed to the intrinsic crystalline habit of the hexagonal system crystals, and the

dx.doi.org/10.1021/cg2010612 | Cryst. Growth Des. 2012, 12, 289−296

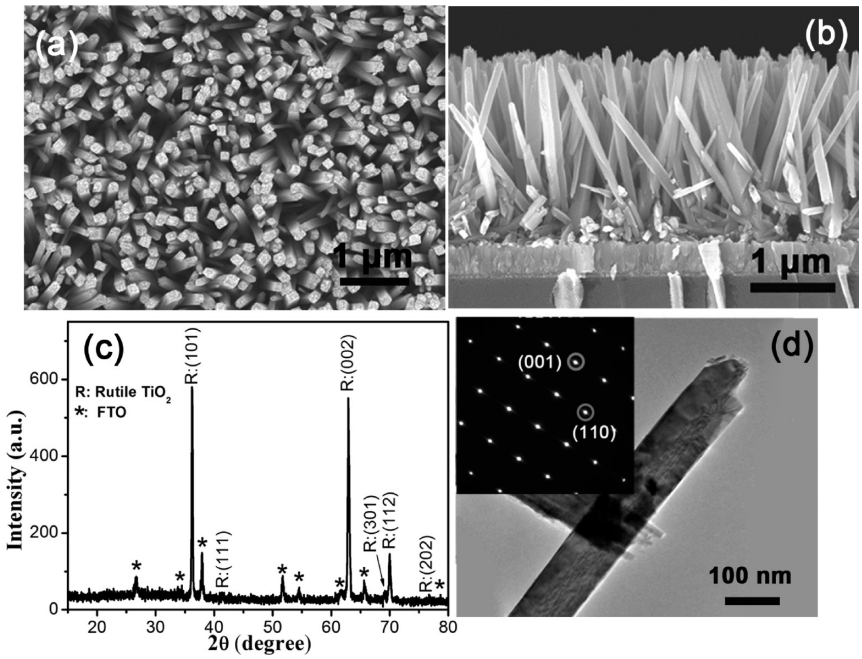

Figure 1. Top-view (a) and side-view (b) SEM images and XRD pattern (c) of TiO_2 nanorod arrays grown on FTO substrate by a hydrothermal method. (d) TEM image of a single TiO_2 nanorod. The inset in panel d shows the SAED pattern of the corresponding TiO_2 nanorod.

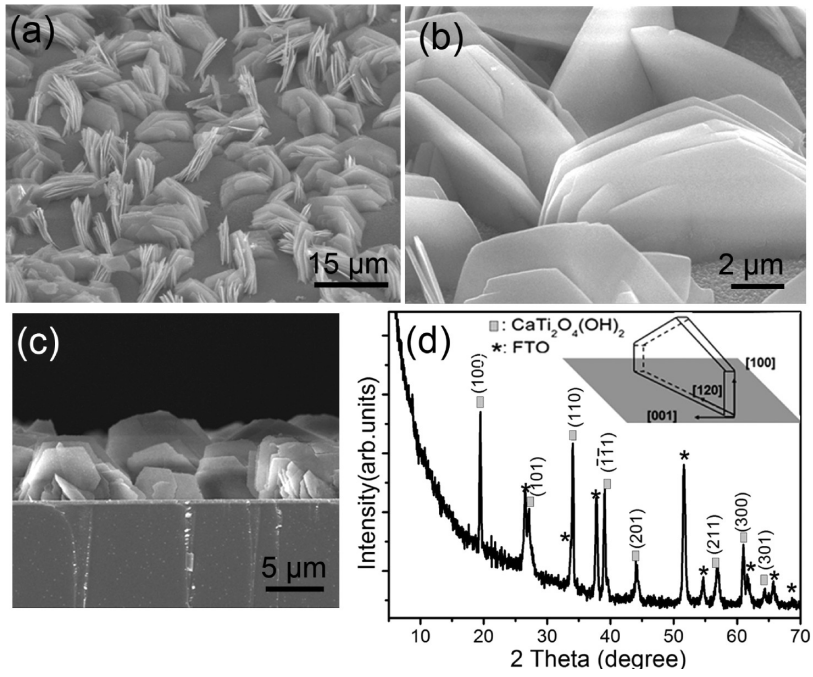

Figure 2. Titled (a and b) and side-view (c) SEM images and XRD pattern (d) of hexagonal nanosheet arrays on FTO substrate obtained by treating the TiO_2 arrays in 10 M NaOH solution at 150 °C for 5 h. The insert in panel d shows the crystal growth model of the hexagonal nanosheet.

growth of $CaTi_2O_4(OH)_2$ nanosheet resembled those shown in the inert of Figure 2d.

To further verify the structure of the hexagonal nanosheets, TEM, SEAD, and EDS measurements were performed. Figure 3 displays the TEM image and corresponding HRTEM and SAED patterns of the multilayer nanosheets. Well-faceted multilayer hexagonal platelets with a smooth surface were demonstrated in Figure 3a. According to the HRTEM image (Figure 3b) and SEAD pattern (Figure 3c), the single-crystalline platelet had a hexagonal structure along the [001] axis. The {100} *d*-spacing was determined to be 0.457 nm, which coincided well with the XRD pattern reflected at 19.5°. The EDS spectrum (Figure 3d) revealed that the platelet contained Ti, Ca, and O (the existence of trace Na in the EDS spectrum could be ascribed to residual NaOH from the precursor). The Ca/Ti and Ti/O atomic ratio was 1:2.1 and 1:2.9, respectively, coinciding with the stoichiometric ratio of $CaTi_2O_4(OH)_2$. All of these results confirmed that the hexagonal platelets formed were single-crystalline kassite. To the best of our knowledge, this was the first time that ordered plateletlike kassite arrays formed on FTO glass substrate.

dx.doi.org/10.1021/cg2010612 | *Cryst. Growth Des.* 2012, 12, 289–296

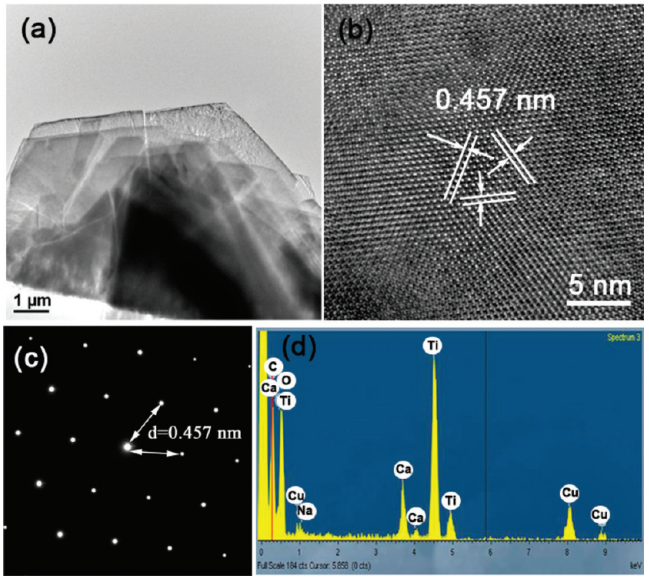

Figure 3. TEM image (a) and corresponding HRTEM (b) and SAED pattern (c) and EDS spectra (d) of the hexagonal nanosheet obtained by treating the TiO_2 arrays in 10 M NaOH solution at 150 °C for 5 h.

A morphology evolution study was conducted to obtain a complete view of the kassite nanosheets formation process. Products obtained by treating the TiO_2 nanorod arrays in 10 M NaOH solution at 150 °C for different times (t) were evaluated by SEM (Figure 4). It was found that there was no appreciable

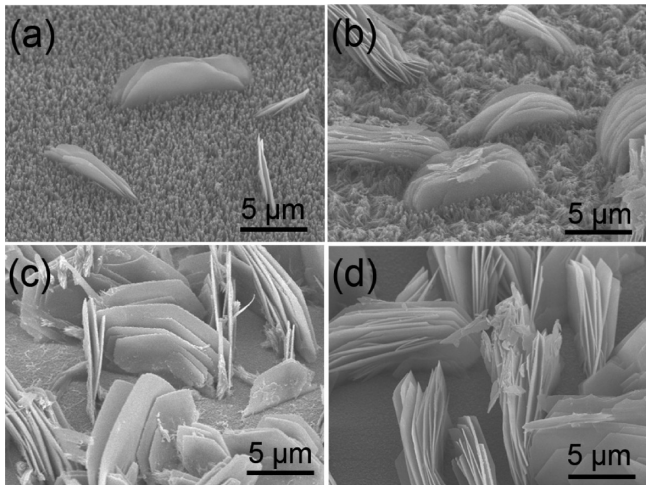

Figure 4. SEM images of the products on FTO substrates obtained by treating the TiO_2 nanorod arrays in 10 M NaOH solution at 150 °C for (a) 2, (b) 3, (c) 4, and (d) 5 h.

change in morphology and crystal structure of the TiO_2 nanorod arrays during the first hour of hydrothermal reaction (not shown in Figure 4). As the reaction proceeds (t = 2 h), the formation of a few nanosheets with a diameter of about 6 μm among TiO_2 nanorods was observed, as evidenced in Figure 4a. These nanosheets stood almost perpendicular to the surface of FTO glass substrate. Increasing the reaction time to 3 and 4 h increased the yields and size of these platelets overall, coinciding with the decrease of TiO_2 nanorods density (Figure 4b,c). By undergoing 5 h of reaction, TiO_2 nanorods disappear entirely, and the final product, pure arrays of nanosheets with mean diameter of 12 μm and thickness of 200 nm, were obtained, as shown in Figure 4d.

The time-dependent products were further characterized by XRD. Figure 5 shows the XRD patterns of the samples obtained

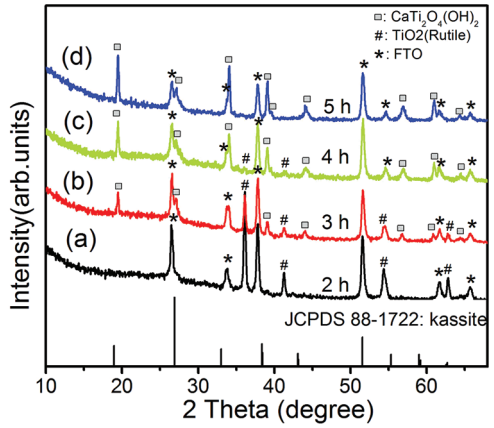

Figure 5. XRD patterns of the products on FTO substrates obtained by treating the TiO_2 nanorod arrays in 10 M NaOH solution at 150 °C for (a) 2, (b) 3, (c) 4, and (d) 5 h.

by treating the TiO_2 arrays in 10 M NaOH solution at 150 °C for 2, 3, 4, and 5 h, respectively. As shown in Figure 5, besides diffraction peaks from rutile TiO_2 and FTO substrate, a weak peak located at 27.0° appeared when the reaction time reached 2 h. This peak could be assigned to the (101) plane of hexagonal kassite. As the reaction time prolonged, the peak intensity of kassite strengthened, whereas the peak intensity of TiO_2 phase decreased, consisting well with the morphology evolution shown in Figure 4. After 5 h of reaction, pure kassite phase can be obtained. According to the SEM and XRD results, it was identified that the formation of kasstie arrays was accompanied by the dissolution of TiO_2 nanorods and no intermediate or transitional products were detected during the hydrothermal process.

Considering that no other sources besides sodium hydroxide aqueous solution were employed in the reaction system, Ca ions in kassite were deduced to come from the glass substrate (with the composition of $Na_2O{\cdot}CaO{\cdot}6SiO_2$). Indeed, after several hours' of reaction, the surface of the naked glass side was coated by a layer of white precipitate, which was proved to be $CaSiO_3$. This provided evidence to support the hypothesis of the involvement of the glass substrate. Therefore, the glass substrate used in our study had a dual role: It acted as the substrate to support the formed arrays and provided a calcium source for the formation of kassite. However, it was found that when the FTO-coated glass substrate was substituted by a bare glass substrate, no kasstite nanosheets but calcium silicate could be obtained on the substrate. Therefore, the FTO coating on the glass substrate also played very important roles in the formation process of kassite nanosheet. First, it acted as a blocking layer to prevent the underneath glass from taking part in the reaction with NaOH solution. Secondary, considering that the lattice mismatch between the (100) planes of FTO (F-doped SnO_2, tetragonal, $a = b$ = 0.4738 nm, and c = 3.188 nm) and kassite (hexagonal, $a = b$ = 0.5245 nm, and c = 0.4784 nm) was very small, it was reasonable to suppose that the FTO coating also enabled the uniform and ⟨100⟩-oriented growth of kassite on glass substrate.

dx.doi.org/10.1021/cg2010612 | Cryst. Growth Des. 2012, 12, 289–296

Scheme 2. Schematic Illustration for the Formation of Kassite Nanosheet Arrays: (a) Generation of Soluble Reactive Groups of Calcium Ions and Hydrolyzed Titanium Species, (b) Sparsely-Distributed Hexagonal Platelets Grown among TiO_2 Nanorod Arrays on the Substrate, (c) More and Larger Hexagonal Platelets Were Formed among the TiO_2 Nanorods, and (d) Complete Dissolution of TiO_2 Nanorods and Formation of Pure Hexagonal $CaTi_2O_4(OH)_2$ Arrays on the Substrate

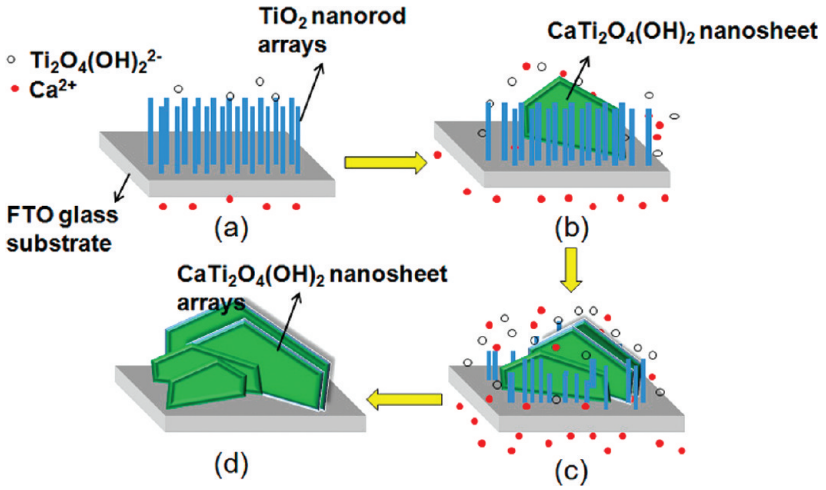

The TiO_2 nanorod arrays were considered to be the Ti precursor from which aqueous titanium species were produced. It was generally recognized in several references[23−26] that the presence of TiO_2 in concentrated NaOH at elevated temperatures would initially lead to its dissolution. As the TiO_2 dissolved, it released Ti^{4+} ions, which formed a variety of aqueous titanium species, such as $Ti_2O_5^{2-}$, $Ti(OH)_2^{2+}$, and $TiO_2(OH)_2^{2-}$.[24] It was not certain in exactly what form these aqueous titanium species existed, but in our study, we think it was some hydrolyzed species, such as $TiO_2(OH)_2^{2-}$. The main chemical reactions that were involved in the formation of $CaTi_2O_4(OH)_2$ were suggested as follows:

$$2TiO_2 + 2OH^- \rightarrow Ti_2O_4(OH)_2^{2-} \quad (1)$$

$$2(Na_2O{\cdot}CaO{\cdot}6SiO_2) + 18NaOH \rightarrow Ca^{2+} + 2OH^- + 11Na_2SiO_3 + CaSiO_3\downarrow + 8H_2O \quad (2)$$

$$Ti_2O_4(OH)_2^{2-} + Ca^{2+} \rightarrow CaTi_2O_4(OH)_2\downarrow \quad (3)$$

On the basis of the above results and deduction, a schematic illustration for the evolution of hexagonal kassite nanosheet arrays is presented in Scheme 2. As the growth of hexagonal nanosheets and dissolution of TiO_2 nanorods occurred simultaneously, the dissolution−nucleation−growth process was suggested to dominate the whole process. In the beginning (Scheme 2a), some Ti−O bonds of the TiO_2 nanorods were broken under the hydrothermal treatment with concentrated NaOH, leading to the formation of $Ti_2O_4(OH)_2^{2-}$ in the vicinity of TiO_2 nanorod arrays.[24,25] Meanwhile, the surface of the naked glass reacted gradually with concentrated NaOH according to reaction 2, releasing Ca^{2+} ions into the solution. The Ca^{2+} ions diffuse to the vicinity of TiO_2 rods and get incorporated with the dissolved titanium specie $Ti_2O_4(OH)_2^{2-}$. The combination of Ca^{2+} and $Ti_2O_4(OH)_2^{2-}$ brought about heterogeneous nucleation and growth of $CaTi_2O_4(OH)_2$. At this stage, the nucleation appeared to preferentially start at the uncovered FTO substrate, because this area was considered to be relatively energetically favorable. After nucleation, the $CaTi_2O_4(OH)_2$ nanosheets grew along the ⟨100⟩ direction to decrease the lattice mismatch with the FTO substrate. Consequently, hexagonal $CaTi_2O_4(OH)_2$ nanosheets, which stood upward, were formed among the TiO_2 nanorods (Scheme 2b). As the reaction time increased, more TiO_2 nanorods were involved in the generation of aqueous titanium species, and more necked sites on FTO substrate were exposed to the solution, inducing more nucleation sites for $CaTi_2O_4(OH)_2$ growth. Because of the increased nucleation sites and reactants [Ca^{2+} and $Ti_2O_4(OH)_2^{2-}$] concentration, more and larger hexagonal $CaTi_2O_4(OH)_2$ platelets were formed among the TiO_2 nanorods (Scheme 2c). The nanosheets stacked layerwise and grew larger with time prolongation, and the TiO_2 nanorods dissolved gradually until they completely disappeared, resulting in well-aligned pure multilayer hexagonal nanosheet structure (Scheme 2d). Unfortunately, it was not clear whether intermediate sodium titanate phases may form. For example

$$3TiO_2 + 2NaOH \rightarrow Na_2Ti_3O_7 + H_2O \quad (4)$$

or

$$2TiO_2 + 2NaOH \rightarrow Na_2Ti_2O_4(OH)_2 \quad (5)$$

It was generally recognized that during the treatment of TiO_2 precursor with concentrated NaOH, lamellar fragments that were the intermediate phase in the formation process of the sodium titanate nanotube material would form.[26−28] In our case, sodium titanates were not detected in any patterns as evidenced by the absence of indicative Bragg reflections at 8.1−8.3 Å in the XRD pattern. However, this did not preclude its involvement in the reaction mechanism of $CaTi_2O_4(OH)_2$ formation, as it was possibly poorly crystalline and likely to be present at low levels.

To further understand the role of Na^+ ions in the synthesis process, we replaced NaOH by KOH, while all other conditions were unchanged. No reflection peaks from $CaTi_2O_4(OH)_2$ were detected from XRD pattern of the KOH-treated product (Figure S1a in the Supporting Information). Besides sharp diffraction peaks from rutile TiO_2, weak diffraction peaks, which can be assigned to $CaTiO_3$ (JSPDS: 81-0562), were observed. This result was also supported by the corresponding SEM image (Figure S1b in the Supporting Information), from which one can see micrometer-sized rectangular prism distributing among the TiO_2 nanorod arrays. In addition, the EDS analysis

dx.doi.org/10.1021/cg2010612 | Cryst. Growth Des. 2012, 12, 289−296

showed that the prisms contained Ti and Ca with a atomic ratio of about 1:1 as presented in Figure S2 in the Supporting Information, confirming that the prism was $CaTiO_3$. Considering that all other conditions such as the temperature and duration time for the KOH-treated sample were identical to those of the NaOH-treated one, we speculated that a high concentration of Na^+ cation was also very crucial in the synthesis of the $CaTi_2O_4(OH)_2$. The Na^+ cation may promote the hydrolysis or dissolution process of TiO_2 (reaction 1), which generated aqueous titanium species. The dissolution of TiO_2 nanorods was retarded obviously when KOH aqueous solution was used, as evidenced by the strong diffraction peak from TiO_2 in Figure S1 in the Supporting Information. Croker suggested that the reaction product [$CaTiO_3$ or $CaTi_2O_4(OH)_2$] between TiO_2 and $CaTiO_3$ or hydrogarnet in alkaline aqueous solution were specific to the relative reactive concentration of calcium species and aqueous titanium species.[29] In the case for KOH adoption, the lower concentration of titanium species relative to that of aqueous calcium led to the formation of $CaTiO_3$, rather than $CaTi_2O_4(OH)_2$.

The mineral kassite $CaTi_2O_4(OH)_2$, being a layered metal hydroxide, was proposed to have some of the same properties as hydrotalcite, a widely recognized double-layered hydroxide. It was considered to be metastable with respect to $CaTiO_3$, transforming to $CaTiO_3$ upon calcinations above 500 °C.[22,29,30] The $[Ti_2O_4(OH)_2]^{2-}$ layers and the location of the Ca atom in $CaTi_2O_4(OH)_2$ is illustrated in Scheme 3. The $TiO_4(OH)_2$ octahedral shared edges in a honeycomb arrangement, giving a layer composition $[Ti_2O_4(OH)_2]^{2-}$. Ca atoms sit above and below the empty octahedral sites in the $Ti_2O_4(OH)_2$ layers, resulting in the CaO_6 octahedral corner-sharing with three $TiO_4(OH)_2$ octahedral from the hexagonal rings on either side.[31] As the lengths of Ca−O bonds (2.302−2.425 Å) were much longer than that of the Ti−O bonds (1.865−2.108 Å), it was possible

Scheme 3. Structure and Arrangement of TiO_6 Octahedra in Kassite [$CaTi_2O_4(OH)_2$] Unit Cells

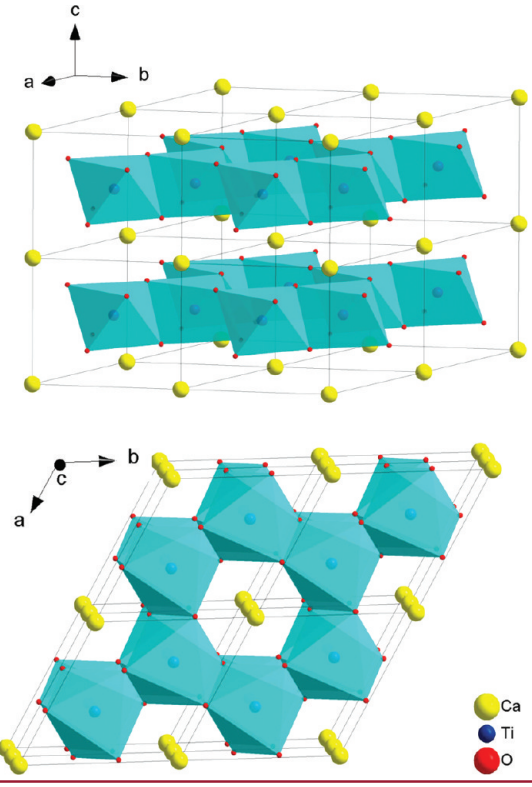

that the Ca^{2+} groups be extracted from the layers. If Ca^{2+} groups were extracted from the layers, TiO_2 would be obtained.

Driven by this rationale, the as-synthesized hexagonal platelike $CaTi_2O_4(OH)_2$ arrays were then hydrothermally treated at 150 °C

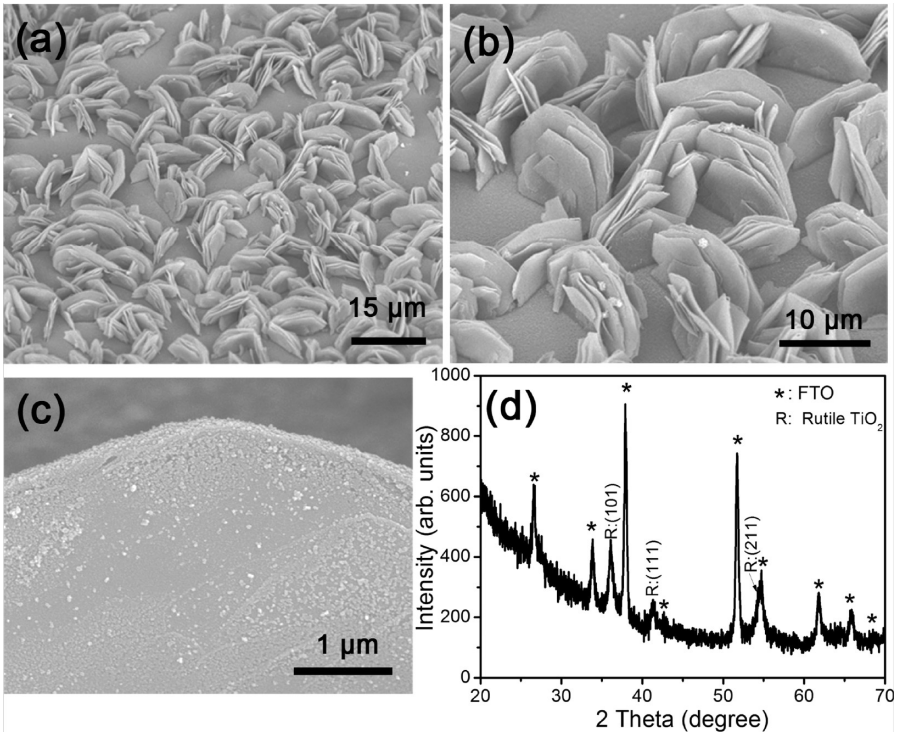

Figure 6. SEM images (a−c) and XRD pattern (d) of the TiO_2 nanosheet arrays obtained by hydrothermally treating kassite nanosheet arrays in 0.1 M HNO_3 aqueous solution at 150 °C for 7 h.

dx.doi.org/10.1021/cg2010612 | Cryst. Growth Des. 2012, 12, 289−296

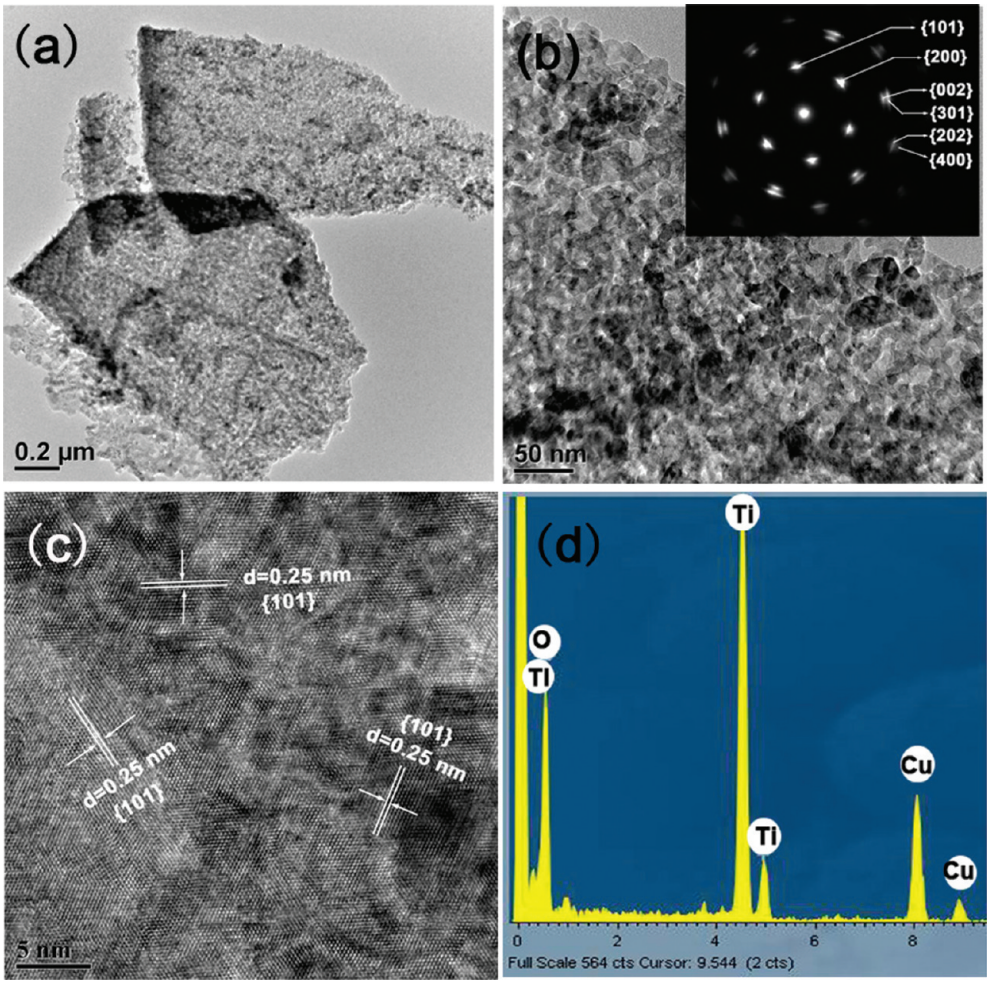

Figure 7. TEM images (a and b) and corresponding HRTEM (c) and EDS spectra (d) of the TiO_2 nanosheet arrays obtained by hydrothermally treating kassite nanosheet arrays in 0.1 M HNO_3 aqueous solution at 150 °C for 7 h. The insert in panel d shows the corresponding SEAD pattern of the nanocrystalline nanosheet.

for 7 h in 0.1 M HNO_3 aqueous solution. SEM images of the corresponding sample (Figure 6a–c) showed that the sizes and morphology of the nanosheet were well maintained during the course of hydrothermal reaction, and the resultant nanosheets took a similar hexagonal shape. The magnified SEM image of the platelet showed that the surface of platelet was grainy and was full with small holes. The XRD spectrum of acid-treated sample (Figure 6d) revealed that the hexagonal $CaTi_2O_4(OH)_2$ phase was completely converted to the rutile TiO_2 phase. The TEM image displayed in Figure 7a showed the presence of pores. It was clear to see that the hexagonal sheet was composed of nanoparticles with diameters in the range of 10–15 nm. Its corresponding SAED pattern (inset of Figure 7b) showed that the overall assembly of TiO_2 had a single-crystalline nature, with the preferred orientation resulting from the fact that the platelet was transformed from the single-crystalline $CaTi_2O_4(OH)_2$ platelet. The HRTEM image (Figure 7c) revealed the lattice fringes spacing of 0.25 nm, in agreement with the d_{101} of the rutile TiO_2. The EDS spectrum recorded on the platelet (Figure 7d) showed that it contained elements of Ti, O, Cu, and C. The Cu and C belonged to the amorphous carbon-coated Cu grid, and Ti and O should be assigned to the platelet. The atomic ratio between Ti and O was estimated to be 1:1.96, which was consistent with that of TiO_2. No Ca element was detected by EDS, indicating that the Ca^{2+} ions were extracted completely from the platelet unit during the course of hydrothermal reaction. The acid treatment enabled the extraction of Ca^{2+} ions and the rearrangement of TiO_6, forming the assembly of TiO_2 nanoparticles with a single-crystalline nature. The transformation of $CaTi_2O_4(OH)_2$ to TiO_2 by the acid treatment can be described as follows:

$$CaTi_2O_4(OH)_2 + 2HNO_3 \rightarrow 2TiO_2 + Ca(NO_3)_2 + H_2O \quad (6)$$

Raman spectroscopy was used to investigate further the local structure of the TiO_2 nanorods, $CaTi_2O_4(OH)_2$, and TiO_2 nanosheets. As shown in Figure 8a, the Raman spectra collected from the TiO_2 nanorods displayed vibration modes located at about 232, 445, and 607 cm^{-1}, which can be uniquely corresponding to second-order Raman scattering, E_g, and A_{1g} of tetragonal structure, respectively. The intensity and peak positions of the above Raman-active phonon modes were in good agreement with the experimental data reported for pure rutile TiO_2 phase.[32] Figure 8b shows the Raman spectrum of the $CaTi_2O_4(OH)_2$ nanosheets. Three Raman modes for hexagonal $CaTi_2O_4(OH)_2$ were found at about 343, 455, and 681 cm^{-1}. The exact assignment of these bands in the Raman spectrum was very difficult due to the lack of reports relating directly the Raman peaks to specific active modes of hexagonal kassite. Figure 8c shows the Raman

dx.doi.org/10.1021/cg2010612 | Cryst. Growth Des. 2012, 12, 289–296

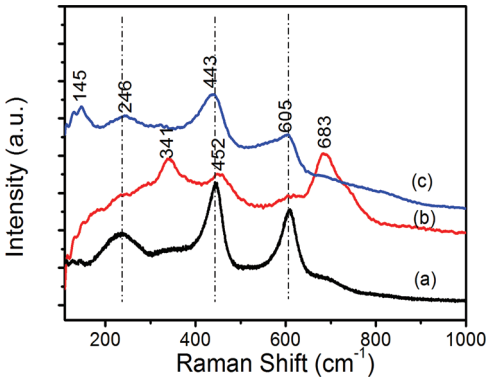

Figure 8. Raman spectra of the TiO_2 nanorod arrays (a), kassite [$CaTi_2O_4(OH)_2$] arrays (b), and rutile TiO_2 nanosheet arrays (c).

spectrum of the acid-treated kassite. Although the spectrum obtained was somewhat broadened and shifted, there was a good match for curve c with that obtained from rutile TiO_2 nanorods, confirming that the product after the acid treatment was of pure rutile TiO_2. Therefore, the weaker band at ~146 cm^{-1} should be assigned to B_{1g} vibration mode of rutile TiO_2.[33] The broadening and red-shifting of Raman bands of the TiO_2 nanosheets could be either or both of two reasons: first, the lower crystallinity of the nanocrystalline TiO_2 platelets as compared to that of the single-crystalline TiO_2 nanorods and, second, the effect of phonon confinement in nanocrystalline TiO_2 platelets, which relaxed the zone-center optical-phonon selection rule and allowed phonon over complete Brillouin zone to contribute to the band broadening.

4. CONCLUSIONS

In this study, we presented a new route for the synthesis of aligned kassite nanosheet arrays on FTO glass substrate. The novel strategy was composed of a direct hydrothermal deposition of vertically aligned TiO_2 nanorods on FTO glass substrate and a hydrothermal reaction of the TiO_2 nanorods in concentrated NaOH aqueous solution. The as-obtained kassite nanosheets showed a single-crystalline nature with their *c*-axis parallel to the substrate. A dissolution–nucleation–growth mechanism was suggested to dominate the whole formation process of kassite. Through an acid treatment of these kassite arrays with HNO_3 solution, TiO_2 nanosheet arrrays with morphology preservation could be produced. The specific advantage of our method is that it provides well-aligned 2D nanosheet arrays of kassite and TiO_2 on the FTO glass substrate, both of which are highly promising for application in catalysts and electroactive or photoactive materials in the future.

■ ASSOCIATED CONTENT

Supporting Information

XRD, SEM image, and EDS spectrum of the sample obtained by treating the TiO_2 nanorod arrays in 10 M KOH at 150 °C for 5 h. This material is available free of charge via the Internet at http://pubs.acs.org.

■ AUTHOR INFORMATION

Corresponding Author

*E-mail: ganxiaoyan@mail.sic.ac.cn.

■ ACKNOWLEDGMENTS

This work was supported by the National Natural Science Foundation of China (No. 51002174, No. 51102661, and No. 51072214) and by the CAS Key Laboratory of Inorganic Coating Materials (No. KLICM-2010-05).

■ REFERENCES

(1) Andersson, M.; Osterlund, L.; Ljungstrom, S.; Palmqvist, A. *J. Phys.Chem. B* **2002**, *414*, 338.
(2) Tada, H.; Suzuki, F.; Ito, S.; Akita, T.; Tanaka, K.; Kawahara, T.; Kobayashi, H. *J. Phys. Chem. B* **2002**, *106*, 8714.
(3) Rothschild, A.; Levakov, A.; Shapira, Y.; Ashkenasy, N.; Komem, Y. *Surf. Sci.* **2003**, *456*, 532.
(4) Armstrong, A. R.; Armstrong, G.; Canales, J.; Bruce, P. G. *Angew. Chem., Int. Ed.* **2004**, *43*, 2286.
(5) Grätzel, M. *Nature* **2001**, *414*, 338.
(6) Kasuga, T. *Langmuir* **1998**, *14*, 3160.
(7) Imai, H.; Takei, Y.; Shimizu, K.; Matsuda, M.; Hirashima, H. *J. Mater. Chem.* **1999**, *9* (12), 2971.
(8) Uchida, S.; Chiba, R.; Tomiha, M.; Masaki, N.; Shirai, M. *Electrochemistry* **2002**, *70*, 418.
(9) Archana, P. S.; Jose, R.; Vijila, C.; Ramakrishna, S. *J. Phys. Chem. C* **2009**, *113*, 21538.
(10) Lei, Y.; Zhang, L. D.; Meng, G. W.; Li, G. H.; Zhang, X. Y.; Liang, C. H.; Chen, W.; Wang, S. X. *Appl. Phys. Lett.* **2001**, *78*, 1125.
(11) Lee, J. C.; Kim, T. G.; Choi, H. J.; Sung, Y. M. *Cryst. Growth Des.* **2007**, *7*, 2588.
(12) Lee, J. C.; Park, K. S.; Kim, T. G.; Choi, H. J.; Sung, Y. M. *Nanotechnology* **2006**, *17*, 4317.
(13) Tian, Z. R.; Voigt, J. A.; Liu, J.; Mckenzie, B.; Xu, H. *J. Am. Chem. Soc.* **2003**, *125*, 12384.
(14) Peng, X. S.; Chen, A. C. *Adv. Funct. Mater.* **2006**, *16*, 1355.
(15) Chatterjee, S.; Bhattacharyya, S.; Khushalani, D.; Ayyub, P. *Cryst. Growth Des.* **2010**, *10*, 12150.
(16) Ito, S.; Ha, N.-L. C.; Rothenberger, G.; Liska, P.; Comte, P.; Zakeeruddin, S. M.; Pechy, P.; Nazeeruddin, M. K.; Grätzel, M. *Chem. Commun.* **2006**, *38*, 4004.
(17) Stergiopoulos, T.; Valota, A.; Likodimos, V.; Speliotis, T.; Niarchos, D.; Skeldon, P.; hompson, G. E.; Falaras, P. *Nanotechnology* **2009**, *20*, 365601.
(18) Qiu, J. J.; Yu, W. D.; Gao, X. D.; Li, X. M. *Nanotechnology* **2006**, *17*, 4695.
(19) Xu, C. K.; Shin, P. H.; Cao, L. L.; Wu, J. M.; Gao, D. *Chem. Mater.* **2010**, *22*, 143.
(20) Feng, X. J.; Shankar, K.; Varghese, O. K.; Paulose, M.; Latempa, T. J.; Grimes, C. A. *Nano Lett.* **2008**, *8*, 3781.
(21) Liu, B.; Aydi, E. S. *J. Am. Chem. Soc.* **2009**, *131*, 3985.
(22) Huang, Y. J; Tsai, M. C.; Chiu, H. T.; Sheu, H. S.; Lee, C. Y *Cryst. Growth Des.* **2010**, *10*, 1221.
(23) Kiatkittipong, K.; Ye, C. H.; Scott, J.; Amal, R. *Cryst. Growth Des.* **2010**, *10*, 3618.
(24) Huang, J. Q; Cao, Y. G.; Wang, M. L.; Huang, C. G; Deng, Z. H.; Tong, H.; Liu, Z. G. *J. Phys. Chem. C* **2010**, *114*, 14748.
(25) Yang, J. J.; Jin, Z. S; Wang, X. D.; Li, W.; Zhang, J. W.; Zhang, S. L.; Guo, X. Y.; Zhang, Z. J. *Dalton Trans.* **2003**, *20*, 3898.
(26) Tsai, C.-C.; Teng, H. S. *Chem. Mater.* **2006**, *18*, 367.
(27) Sun, X. M.; Li, Y. D. *Chem.—Eur. J.* **2003**, *9*, 2229.
(28) Bavykin, D. V.; Parmon, V. N.; Lapkin, A. A.; Walsh, F. C. *J. Mater. Chem.* **2004**, *14*, 3370.
(29) Croker, D.; Loan, M.; Hodnett, B. K. *Cryst. Growth Des.* **2009**, *9*, 2207.
(30) Li, X. B.; Zhou, Q. S.; Wang, H. Y.; Peng, Z. H.; Liu, G. H. *Hydrometallurgy* **2010**, *104*, 156.
(31) Grey, I. E.; Mumme, W. G.; Pekov, I. V.; Pushcharovsky, D. Y. *Am. Mineral.* **2003**, *88*, 1331.
(32) Nosheen, S.; Galasso, F. S.; Suib, S. L. *Langmuir* **2009**, *25*, 7623.
(33) Mattsson, A.; Sterlund, L. *J. Phys. Chem. C* **2010**, *114*, 14121.